Australian Government
Department of Defence
Defence Science and
Technology Organisation

On the Design of Multistatic Sonobuoy Fields for Area Search

S. Ozols and M.P. Fewell

Maritime Operations Division
Defence Science and Technology Organisation

DSTO-TR-2563

ABSTRACT

The detection performance of a wide variety of multistatic buoy field layouts is compared using a recently developed method. The analysis applies to large area search; no consideration is given to situations where the search area can be covered with a few sonobuoys. The preferred layout depends on the ratio C_R of receiver cost to source cost. At $C_R \sim 1$, the best performing layout is a square grid; near $C_R = 0.5$ it is hexagonal; for $C_R \sim 0.1$, several layouts give comparable performance. These results hold for three different schematic monostatic detection-probability curves, ranging from almost a cookie cutter to a shape with a low-p_d tail out to several times the range of the day.

Published by

Maritime Operations Division
DSTO Defence Science and Technology Organisation
PO Box 1500
Edinburgh South Australia 5111 Australia

Telephone: (08) 7389 5555
Fax: (08) 7389 6567

AR-015-023
June 2011

APPROVED FOR PUBLIC RELEASE

On the Design of Multistatic Sonobuoy Fields for Area Search

Executive Summary

The impending introduction of a multistatic capability into service on the AP-3C aircraft and the multistatic requirements of Project AIR 7000 give rise to a requirement for performance analysis of multistatic sonobuoy fields. While application of the full arsenal of techniques for acoustic propagation modelling may be the eventual goal, there is also a need for approximate methods that are accurate enough to give guidance on the design of sonobuoy fields and flexible enough to be applicable to as wide a variety of layouts as possible. This report presents the results of such an analysis.

The modelling uses a recently developed method for relating multistatic sonar performance to the performance of similar sonars operated monostatically. It allows multistatic coverage area to be determined relative to the corresponding monostatic coverage area with modest computational effort. That is, multistatic coverage areas are expressed as multiples of R_0^2, the square of the monostatic range of the day, thereby allowing very different buoy field designs to be compared quantitatively without having to determine the actual value of R_0.

We also adopt a novel definition of 'coverage area', basing it on track-initiation probability using a 3-in-5 initiation rule, rather than detection probability. Not only does this take some indirect account of the impact of false detections, it also provides a systematic and theoretically rigorous method for combining detection probabilities from many receivers. Our metric of field performance is based on the maximum separation between sonobuoys such that the track-initiation probability does not fall below 50% anywhere in the field, other than in residual blind zones around each buoy. To allow for the geometric effects of differently shaped layouts, we express the metric as a maximum coverage area per source, called max CATING per source (CATING: Coverage Area based on Track Initiation and No Gaps).

We examine a total of 27 multistatic layouts, mainly variations on a square grid, but including triangular, hexagonal and octagonal designs. The analysis applies to large area search; we do not consider scenarios where the search area can be covered with a few sonobuoys.

In view of the concern over cost among sonobuoy users, the final measure of performance is field cost per unit CATING, parameterised by the ratio of receiver cost to source cost. Costs include only the cost of the sonobuoys expended; we do not attempt to quantify aircraft flying costs in laying complicated patterns, nor do we consider the cost of monitoring receiver-rich sonobuoy fields.

The analysis was carried out for three different schematic shapes of monostatic single-ping detection-probability curve, ranging from almost cookie-cutter to a curve with a low-p_d tail stretching out well beyond the monostatic range of the day R_0, which we take to be the range at which $p_d = 0.5$.

The following results were achieved for all three p_d curves, and so should apply for a wide range of real-world p_d curves:

- For receiver cost equal to source cost, such as when using an explosive source, a straightforward square grid is the most cost effective layout.
- For a receiver cost of half the source cost (approx. BARRA with AN/SSQ-125), the hexagonal layout is best.
- For a receiver cost of one tenth the source cost (e.g. DIFAR with AN/SSQ-125), there are several layouts with similar performance: we dub them argyle shift, hexagonal plus and chessboard plus with posts. Chessboard plus is perhaps the easiest to lay.

None of these layouts involves 'posts' (i.e. collocated source–receiver pairs) alone. Such 'P fields' have one receiver per source; the comparable separated layout is the square grid, an 'SR field', which we find always outperforms the P-field layouts.

Authors

S. Ozols
Maritime Operations Division

Sylvia Ozols took up a summer vacation scholarship at DSTO in 2009–10. She had just completed her third year in a Bachelor of Mathematics & Computer Science at the University of Adelaide with the intention of going on to postgraduate study in Pure Mathematics.

M.P. Fewell
Maritime Operations Division

Matthew Fewell joined DSTO in 2001, coming from an academic physics background. He has worked and published in experimental nuclear structure physics, gaseous electronics, atom–photon interactions including coherent effects, laser physics, plasma processing of materials, the conceptual underpinnings of network-centric warfare and its modelling (including cognitive issues), human-in-the-loop experimentation, and weapon–target allocation in ship air defence. He is at present engaged in anti-submarine warfare operations research, with a focus on networking effects and multi-platform operations.

Contents

Figures

Tables

Acronyms

CATING	coverage area based on track initiation and no gaps
P field	sonobuoy field composed solely of posts (i.e. collocated source–receiver pairs)
PR field	sonobuoy field composed of posts and receivers only
SPR field	sonobuoy field containing all three types of node
SR field	sonobuoy field composed of isolated sources and receivers only

1. Introduction

Considering the endless possibilities that could be suggested and implemented as ways to lay out a field of multistatic sonobuoys we need a method of determining which field layout is best, and why. In this report we apply a recently developed method for quantitatively analysing how 'good' a field layout is [1,2] to a total of 27 buoy-field designs in order to determine the optimal layout according to the model.

Sensor cost is a major concern in sonobuoy operations. As Traweek and Wettergren put it [3]:

> 'Reducing … costs has rightfully been a dominant theme throughout the 50 year history of sonobuoy design, production and logistical support, one that has been motivated by vast operational experience …'

In multistatic buoy fields, sources can be considerably more expensive than receivers, so the area covered per source would be a useful metric. Receivers, however, are not free and covering an area entirely with receivers is not a feasible option. Accordingly, we calculate the number of receivers per source for each field design and the final measure of performance: cost per unit area in covering a large search area, where 'coverage area' is defined in a novel way involving track initiation and the absence of coverage gaps, as described in section 2.2.

2. Method

This study uses a recently developed method for relating monostatic and multistatic detection performance. The method is summarised in the following subsection and detailed in companion reports [1,2]. Section 2.2 describes the metrics and section 2.3 gives details of the field layouts explored.

2.1 Relating Monostatic and Multistatic Detection Ranges

We determine our multistatic range from the equivalent monostatic range. In short, as others have done (e.g. [4–7]), we calculate an equivalent monostatic range R_{equiv} as [1]

$$R_{\text{equiv}} = \sqrt{R_{\text{ST}} R_{\text{RT}}}\ , \tag{1}$$

where R_{ST} is the source–target distance and R_{RT} is the receiver–target distance in the multistatic geometry. This can be used in a monostatic detection probability curve (p_d curve) to determine the multistatic probability of detection. A correction for absorption is applied, leading to a decrease in R_{equiv} which, though increasingly important as range increases [2], remains small over the ranges of interest here. We investigate each field layout with three different schematic p_d curves — exponential:

$$p_d(R) = \begin{cases} 10^{-0.30103R/R_0} & R \geq R_b \\ 0 & R < R_b, \end{cases} \tag{2}$$

and Fermi with high and low values of the diffusivity b:

$$p_d(R) = \begin{cases} \dfrac{1}{1+10^{(R/R_0-1)/b}} & R \geq R_b \\ 0 & R < R_b. \end{cases} \tag{3}$$

In Equations (2) and (3), R_0 is the 'range of the day', the range at which p_d = 0.5, and R_b is the radius of the 'blind zone', an area with zero probability of detection immediately around each monostatic sensor. In the bistatic case, the blind zone is an ellipse with the source and receiver at the foci [2]. We handle multistatics by considering each source–receiver pair in turn.

All p_d curves used are displayed in Figure 1. The reasoning behind using several curves is to explore whether the p_d curve makes a difference in which layouts are best. The three curves were chosen to show a wide range of tailing, from almost none in the low-diffusivity Fermi case to very long in the exponential case, since previous work had shown the important influence of tailing on performance in networks of sonars [8]. Throughout this study we retain the same range of the day R_0 ensuring we compare only the differences in p_d-curve shape.

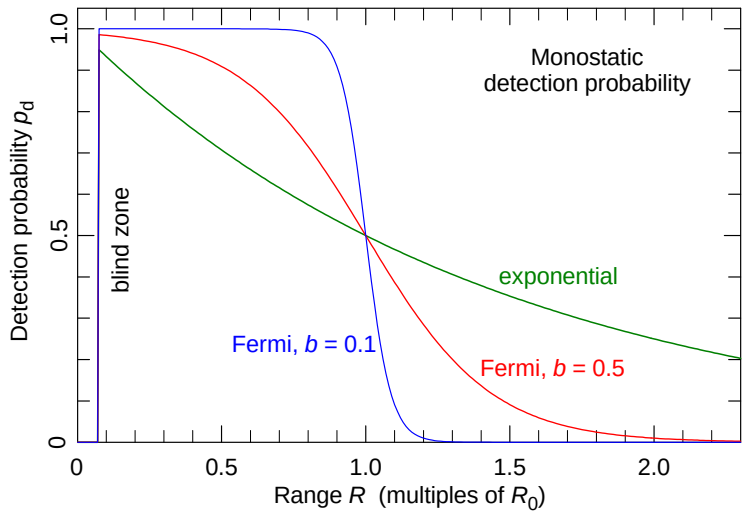

Figure 1: The three p_d curves used as models of monostatic detection

2.2 Metrics

As mentioned in section 1, the measure of performance that we use to determine the 'best multistatic sonobuoy layout' is cost per unit area covered. We define 'coverage area' in a non-standard way, as described in section 2.2.1. We focus on the area that a single source covers when part of a large buoy field, and we determine the number of receivers for each source. These quantities depend on the details of the layout. From that we determine the cost of each layout per unit area, taking into account the possibility that receiver cost and source cost may be different.

The centre of a sonobuoy field can have very different coverage characteristics from the same section of the pattern near the edge of the field. In order to regard a field spacing as acceptable we require only that the interior of the sonobuoy field is adequately covered, while ignoring edge effects, since these can vary between layouts. In this way we are considering what the field would look like were it 'laid out to infinity'—obviously impractical but a useful point of view for comparing layouts over large areas. We have given no consideration to which layout would be best if only a few sonobuoys were needed to cover an area.

2.2.1 Coverage Area per Source Based on Field Track-Initiation Probability

Coverage area is usually defined in terms of detection probability—the area over which p_d is greater than 50%, say—but we choose to define it in terms of track initiation probability p_{ti} for reasons argued in detail elsewhere [2,8,9]. Of those reasons, perhaps the most important for the present study concerns the fusion of data from multiple receivers. Even current practice with monostatic sonobuoys treats the whole field as one detector from the point of view of tracking. That is, it is not the case that, to start a track, three detections are required in five pings (say) of a single sonobuoy. The three detections may come from any sonobuoy. They might, for example, occur in a single cycle of pings of all the buoys in the field. With a multistatic field, it is possible for a single ping to produce detections in three different receivers, thereby fulfilling the track-initiation criterion. Using track-initiation probability takes this into account. We use the 'centralised multistatic' network architecture of reference 2. Not only does this give the best performance, in terms of coverage area, of the architectures considered in reference 2, it also corresponds to the way in which we expect a multistatic sonobuoy field would be operated.

Thinking in terms of p_{ti} also takes some account of false detections. As in earlier studies [2,8], we do not model false detections explicitly, but rather rely on the filtering effect of the track initiation step to mitigate their impact.

In summary, the track-initiation probability employed here is the probability of three detections somewhere in the field after *every source* in the field has pinged five times each. The method of calculating it from detection probability is derived in reference 1.

Having settled on the type of probability to be used, two issues remain to turn it into a metric: what value to choose and how to apply it. As to the value, a 50% probability cut-off

is often considered to be standard [9], and we adopt it here. Hence, if the calculated p_{ti} is above 50% then we consider that point in the field covered; otherwise, it is a gap. It would perhaps be normal to apply this by calculating the maximum coverage area for each layout, but the concept of 'maximum coverage area' does not sit easily with the concept of an infinite field. Instead, therefore, we adopt a 'no gaps' approach as our fundamental metric: we determine the maximum separation between sonobuoys for which there is no gap in coverage in the interior of the field. The exception is the residual blind zones formed by the intersection of the blind zones of all bistatic pairs; we do not consider the blind zone in the immediate vicinity of each source and receiver to be a gap. Figure 2 illustrates fully covered and unsatisfactorily covered fields.

Upon placing the sources at their maximum distance apart consistent with full coverage, we algebraically calculate the area covered per source. We do not subtract the area of the residual blind zones. The result is called max CATING (Coverage Area based on Track Initiation and No Gaps) per source. It is determined to the nearest $0.1 R_0^2$ for the Fermi p_d curves and to the nearest multiple of R_0^2 for the exponential p_d curve, because of the significantly larger area values in that case.

2.2.2 Number of Receivers per Source and Max CATING per Sonobuoy

Despite the relative cheapness of receivers, as compared with sources, we should not consider them to be free. To take account of this we count the number of receivers needed per source by inspecting each particular layout. For this purpose, it is helpful to determine the 'unit cell' of a layout. This is the basic unit of the pattern which, when repeated, generates the layout. These are shown in section 2.3. Values of number of receivers per source are tabulated in section 2.3.4.

CATING per source neglects receiver cost—there is no penalty for adding more receivers. An opposite view is provided by 'CATING per sonobuoy'. We count each source and each

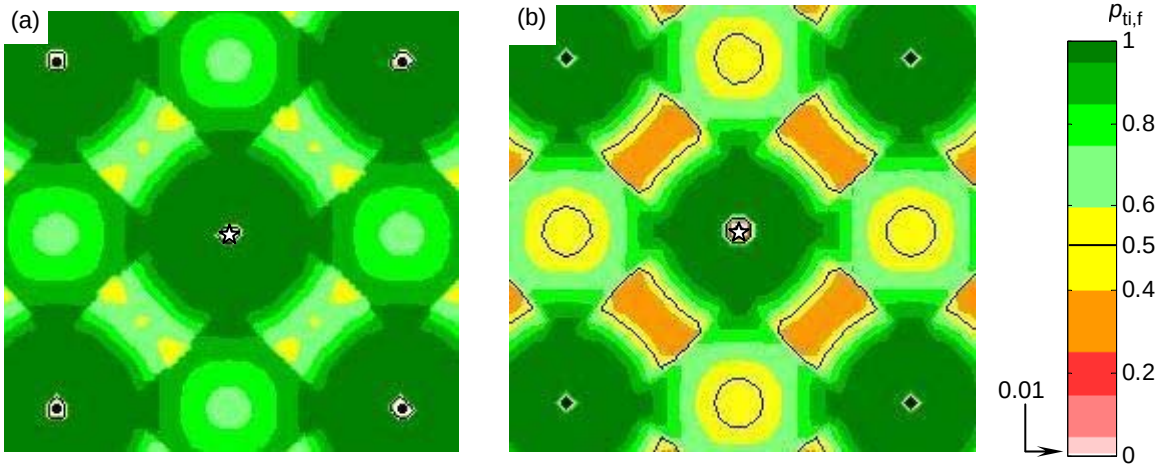

Figure 2: Multistatic field (a) fully covered and (b) unsatisfactorily covered. Contours of field track initiation probability are shown for a source and 4 receivers in the interior of a large square array. Source: ☆, receivers: ●. The 50% contour is shown by a line and the contour fill is white below $p_{ti,f}$ *= 1%. Residual blind zones (small regions in white) can be seen close to each sonobuoy.*

receiver as a separate sonobuoys, regardless of whether they are collocated. That is, CATING A_b per buoy is related to CATING A_S per source by

$$A_b = \frac{A_S}{1 + n_R}, \tag{4}$$

where n_R is the number of receivers per source.

2.2.3 Field Cost per Unit CATING

CATING per source treats receivers as free; CATING per sonobuoy as if they are as expensive as sources. It is clearly desirable to scale between these two. This line of thought leads to our final measure of performance, the field cost C_f per unit CATING:

$$C_f = \frac{1 + n_R C_R}{A_S}, \tag{5}$$

where n_R is the number of receivers per source, C_R is the cost of a receiver and A_S is the max CATING per source. All costs are given as a fraction of the cost of a source and areas are measured in units of R_0^2 (square of the monostatic range of the day). We plot field cost per unit CATING against receiver cost to determine which layouts are most cost effective. These plots can be found in section 3.3.

2.3 Field Layouts Studied

The options for field layouts are almost endless. We begin with a very simple and frequently studied field layout—interleaving square grids of sources and receivers. This design is shown in Figure 3(a), which also shows the unit cell of the pattern. An obvious variation of this is to collocate sources and receivers to give so-called 'posts'—Figure 3(b).

The reason for considering other layouts is the relative cost of receivers to sources. Both square grid and square collocated have one receiver for each source, as the unit cells show. If receivers are cheaper than sources, the aim would be to find layouts with a ratio of receivers to sources greater than 1:1 without degrading too much the good CATING per source achievable by the square grid.

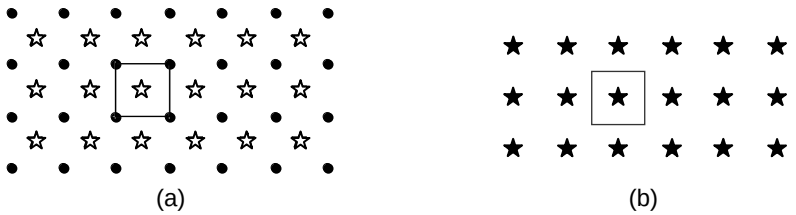

Figure 3: (a) 'Square grid', (b) 'square collocated'. Sources: ☆, receivers: ●, 'posts' (collocated sources and receivers): ★. The unit cell of each pattern is shown.

2.3.1 Rectangular Layouts

Recently a commercial supplier of multistatic sonar processing systems suggested the layout in Figure 4. It achieves four receivers per source by removing every second row and every second column of sources from the square grid. (Figure 4 shows how the four closest receivers to a source are now wholly inside the unit cell instead of being shared with neighbouring cells, as in Fig. 3a.)

When the max CATING of the quarter sources layout is determined (see section 3.1 for coverage plots) gaps first appear near the corners of the unit cell. Three different ways of filling in these gaps suggest themselves:

- placing receivers in the gaps—Figure 5(a),
- shifting alternate rows by half a unit cell so that the corners four unit cells do not meet—Figure 5(b),† and
- placing sources in the gaps—Figure 5(c).

The last reduces the number of receivers per source, but this should be offset by a larger possible sensor separation. Whether it is enough is shown in section 3.3.

Continuing in the same vein, we examine where gaps appear in the three layouts in Figure 5. In these gaps we place receivers, simultaneously creating a larger receiver to source ratio and increasing the max CATING per source. Figure 6 shows the results. With this, the sensor density of the square grid is restored. That is, for equal inter-sensor spacing, the layouts of Figure 6 have the same number of sensors per unit area as the square grid of Figure 3(a), but varying numbers of sources are replaced with receivers in a systematic manner (as opposed, for example, to sources being randomly selected for replacement).

2.3.2 Hexagonal and Octagonal Layouts

In order to increase the number of receivers per source and capitalise on possible benefits to be gained from symmetry, two other basic designs were considered: hexagonal and octagonal—Figure 7(a,b). For completeness, we include the hexagonal collocated layout

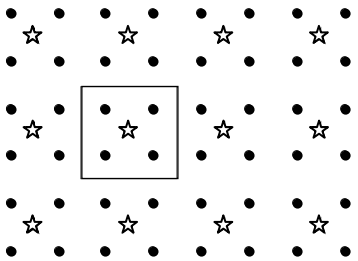

Figure 4: 'Quarter sources' layout, as recently suggested by a commercial supplier of sonar processors. The unit cell is again shown.

†The unit cell for quarter sources shift (Fig. 5b) is the same as for quarter sources (Fig. 4), although the patterns are different. This highlights that our usage of the term 'unit cell' is not the same as in crystallography. For our purposes, it is sufficient that the unit cell shows the area covered by a source and allows one to count the number of receivers per source correctly.

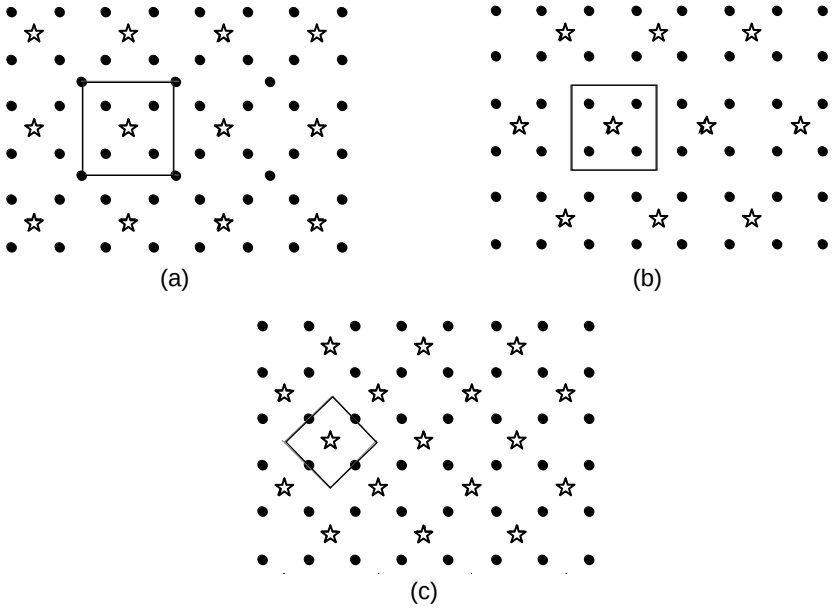

Figure 5: Three variants on the quarter sources layout: (a) 'quarter sources plus', (b) 'quarter sources shift', (c) 'chessboard'

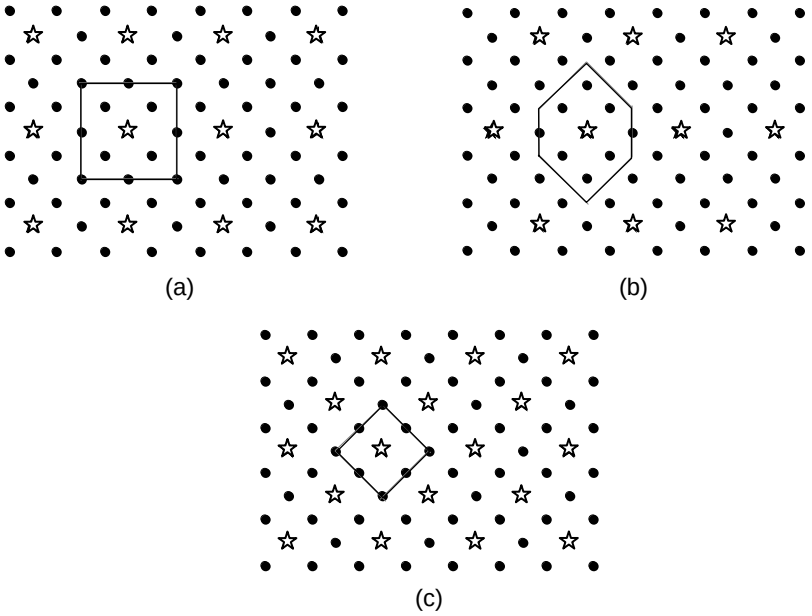

Figure 6: Three further developments of quarter sources: (a) 'argyle', (b) 'argyle shift' and (c) 'chessboard plus'

(Fig. 7c) since, although not expected to perform well, it is one of the regular tilings of the plane.

The hexagonal layout turns out to be the most promising, so, as above, we also tested a layout with extra receivers added where gaps first appear as the inter-sensor spacing is increased—Figure 7(d). The layouts of Figure 7(a,b,d) approximate the 'circle-tac' layout of Grimmett *et al.* [10], though without the multiple sources at the centre of the unit cell.

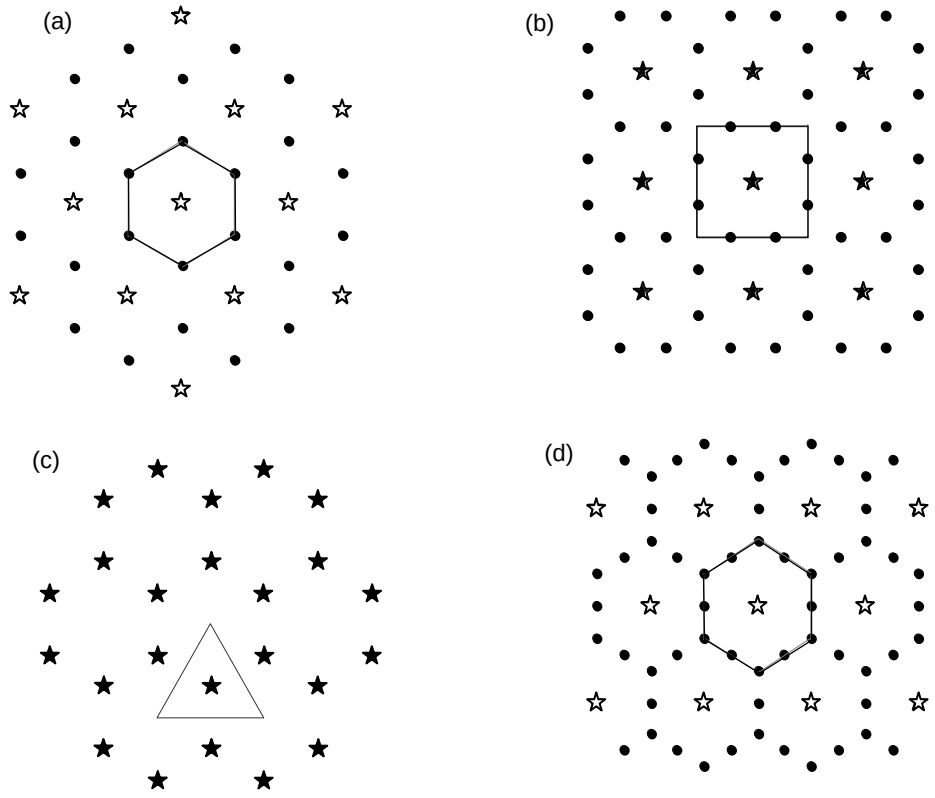

Figure 7: (a) 'Hexagonal', (b) 'octagonal', (c) 'hexagonal collocated', consisting solely of posts, and (d) 'hexagonal plus' layouts. Sources: ☆, receivers: ●, posts (collocated sources and receivers): ★.

2.3.3 Triangular Layouts

In a companion report [2] we consider collocated source–receiver pairs arranged in a triangular pattern—Figure 8(a). This has the same number of receivers per source as the square grid, and turns out not to perform as well (section 3.1), but we include it here as a baseline. It prompts the question of whether a triangular grid with sources and receivers separated might do better. The most symmetric pattern would have a source at the centroid of a triangle of receivers—Figure 8(b). This is not promising because it has two sources per receiver; that is, 0.5 receivers per source, the lowest number of all the layouts considered. (It is in fact the hexagonal pattern with sources and receivers interchanged.)

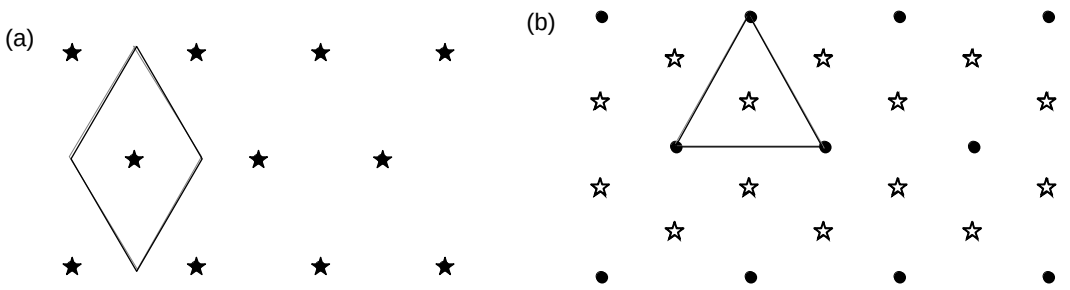

Figure 8: (a) 'Triangular collocated' and (b) 'triangular'

2.3.4 Receivers per Source

The number of receivers per source is listed in the middle column of Table 1 for each of the layouts in Figures 3–8, obtained by inspecting the unit cells. Since receivers cost less than sources, it seems useful to test whether max CATING per source could be improved by adding an extra receiver at the location of every source; that is, by converting the isolated sources into posts. This increases the number of receivers per source by one for each layout, as shown in the right-hand column of Table 1. (All receivers in the collocated layouts are already incorporated into posts, so there are no corresponding layouts without receivers at sources, and hence no entry for the these layouts in the middle column.)

3. Results

3.1 Max CATING per Source

We first present a selection of the coverage area plots, followed by a compilation of the values of max CATING per source for each layout and each p_d curve.

All layouts have a larger coverage area for the high diffusivity p_d curve than the low, and the exponential p_d curve is far better again. This is to be expected as the strength of multistatics lies in the 'tail' of the p_d curve [2]. So, for display purposes we group plots by p_d curve—Figures 9–11. All of the layouts shown in this section are plotted at the maximum sensor spacing that gives full coverage, as described in section 2.2.1. Note the much

Table 1: Number of receivers per source for the layouts as shown in Figures 3–8 ('no receivers at sources') – apart from the collocated layouts – and with an extra receiver collocated at each source ('with posts')

Layout	No receivers at sources	With posts
argyle shift	7	8
argyle	7	8
hexagonal plus	5	6
quarter sources plus	5	6
quarter sources	4	5
quarter sources shift	4	5
octagonal	4	5
chessboard plus	3	4
hexagonal	2	3
chessboard	2	3
square grid	1	2
triangular	½	1½
triangular collocated	–	1
square collocated	–	1
hexagonal collocated	–	1

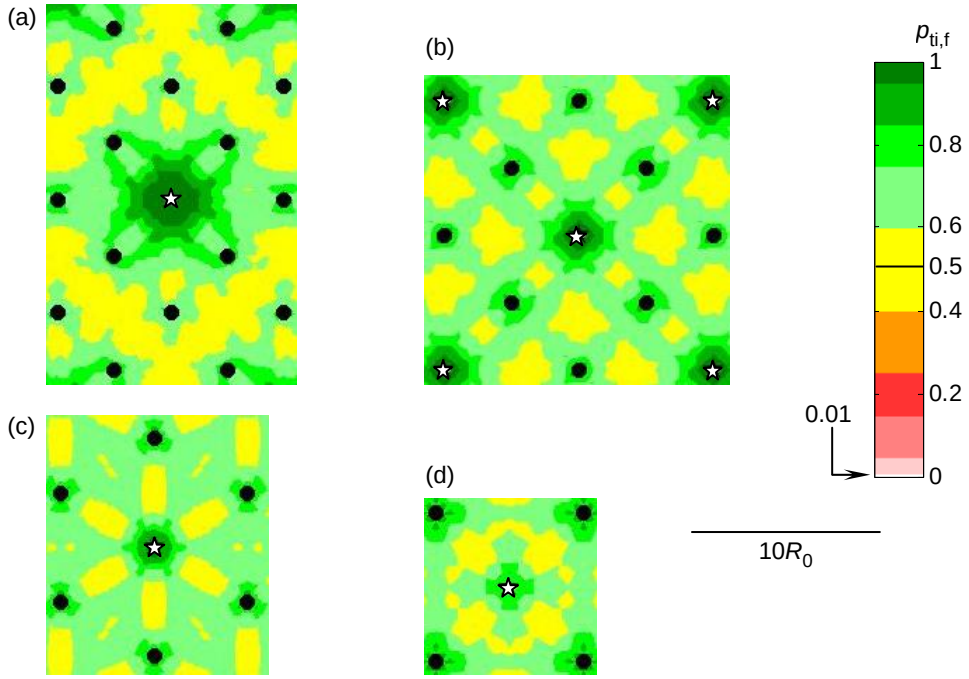

Figure 9: Contours of track-initiation probability at maximum field spacing with the exponential p_d *curve: (a) argyle shift, (b) chessboard plus, (c) hexagonal, (d) square grid. As in Figures 2–8, source locations are shown by open stars and receiver locations by filled circles. All panels are to the same scale (note that the scale bar shows* $10R_0$*).*

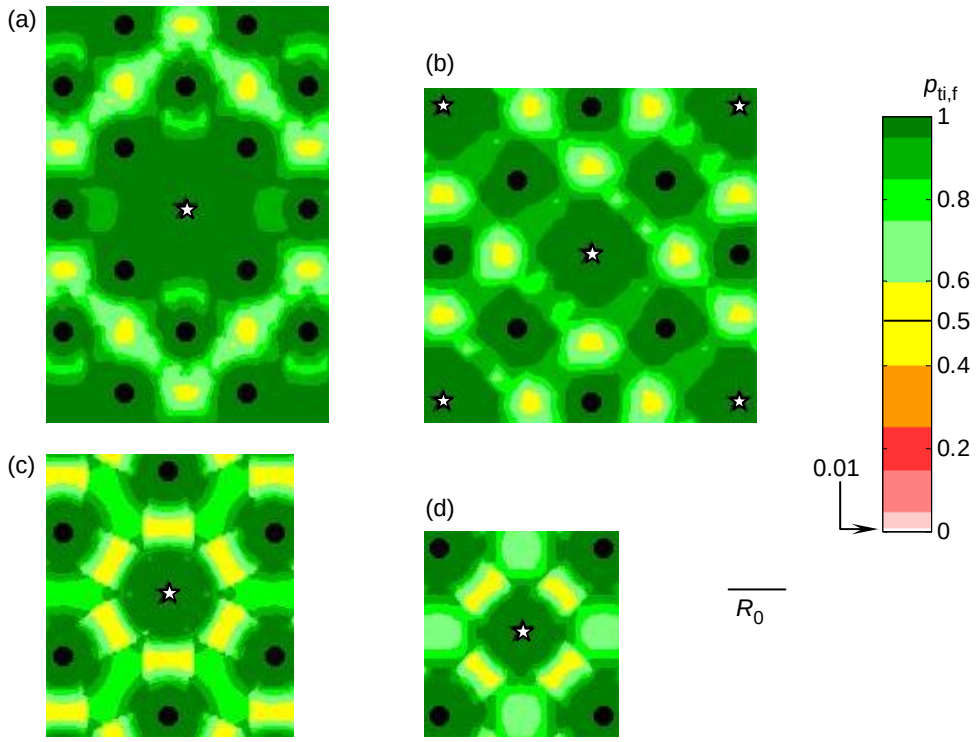

Figure 10: Like Figure 9, but for the Fermi ($b = 0.5$) p_d *curve. (Note that the scale bar shows* R_0*, not* $10R_0$ *as in Figure 9.)*

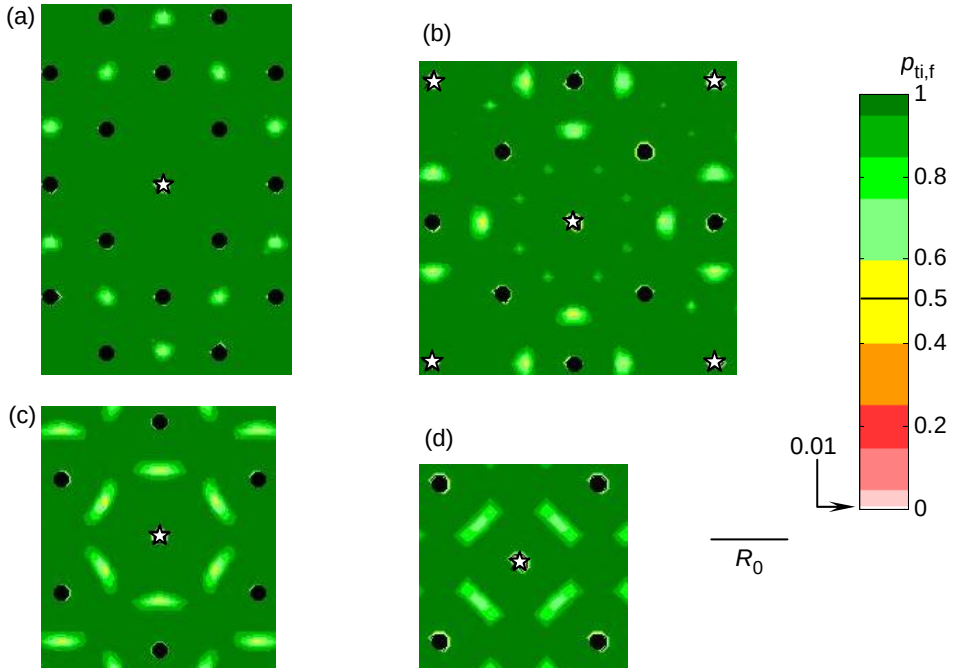

Figure 11: Like Figure 10, but for the Fermi (b = 0.1) p_d *curve*

larger coverage with the exponential p_d curve — the scale bar in Figure 9 marks *ten times* the monostatic range of the day R_0. On the other hand, the average p_{ti} over the field is lower with the exponential than with the Fermi p_d curves. This is to be expected from the shape of the p_d curves (Fig. 1).

The layouts shown in Figures 9–11 are among the better ones. For comparison, Figure 12 shows some poorer performing layouts.

The max CATING per source is the area of the unit cell when sensors are spaced as far apart as possible consistent with full coverage. Values are shown in Figures 13–15 for the three p_d curves. These figures are plotted to emphasise the relationship between the lay-outs as depicted in section 2.3 and those with an extra receiver at each source location. Naturally, adding the extra receiver is never worse than not having receivers at the sources. The extra receiver contributes least with the low diffusivity Fermi p_d curve (Fig. 15), which is a reflection of its almost-cookie-cutter nature.

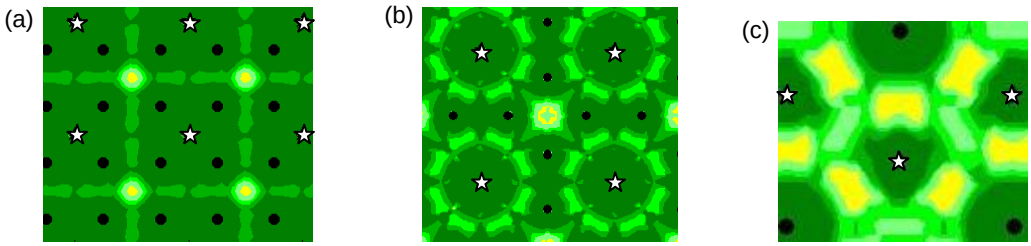

Figure 12: Some of the poorer performing layouts at their maximum field spacing (Fermi p_d *curve,* b = *0.5): (a) quarter sources, (b) octagonal, (c) triangular. The panels are not on the same scale.*

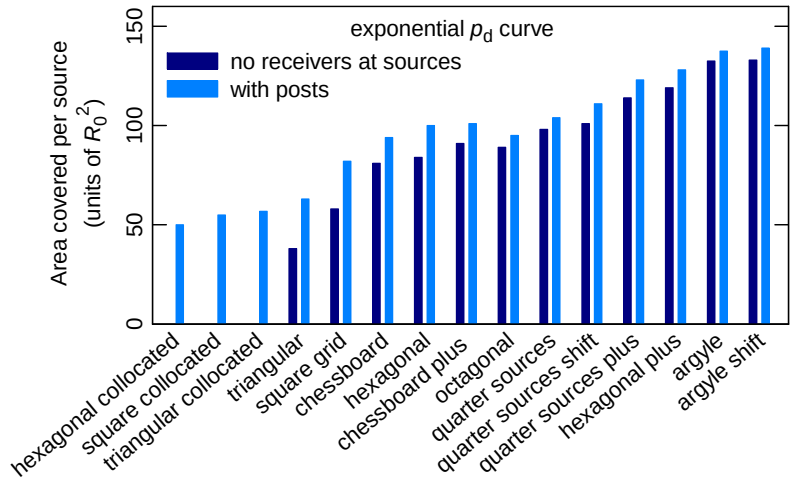

Figure 13: Max CATING per source for the exponential p_d *curve*

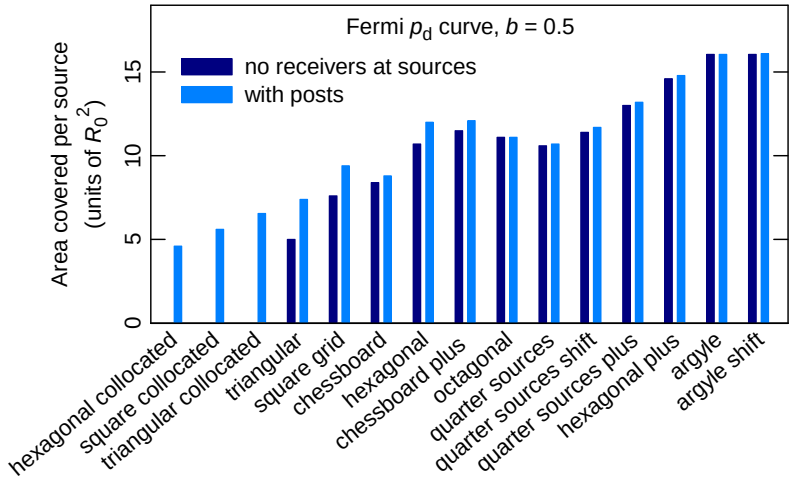

Figure 14: Like Figure 13, but for the high diffusivity Fermi p_d *curve. The order of the layouts is the same as in Figures 13 and 15.*

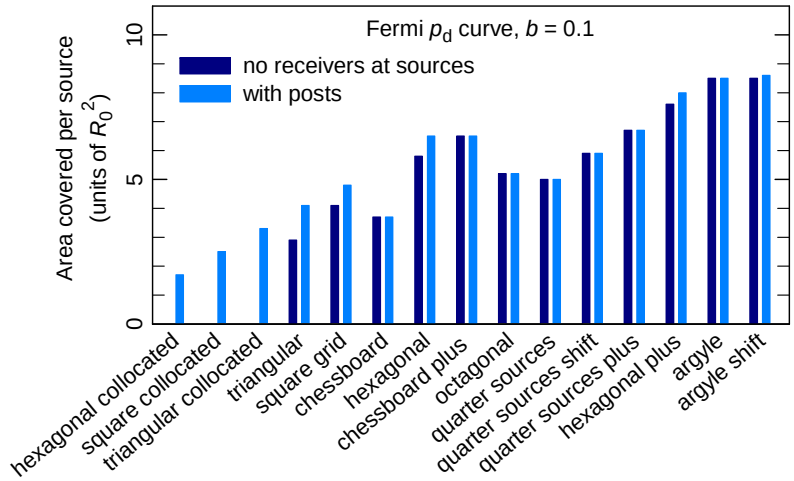

Figure 15: Like Figure 13, but for the low diffusivity Fermi p_d *curve. In this case, placing an extra receiver at the source rarely has much effect.*

Figures 13–15 show a distinct similarity in the ranking order of the layouts across all three p_d curves. Although they are not identical, it gives some indication that changing the p_d curve does not change the best layout too much. To see more completely the extent of variations as the shape of the p_d curve changes, Figure 16 collects the results in Figures 13–15 into one diagram. It is only when the connecting lines in Figure 16 cross that the layout ranking changes between p_d curves.

Figure 16 shows that variants of the argyle layout perform best, on this metric, for all three p_d curves. The hexagonal plus layouts also do well, particularly for the Fermi p_d curves. As the degree of tailing in the p_d curve increases, the quarter-source variants move up the

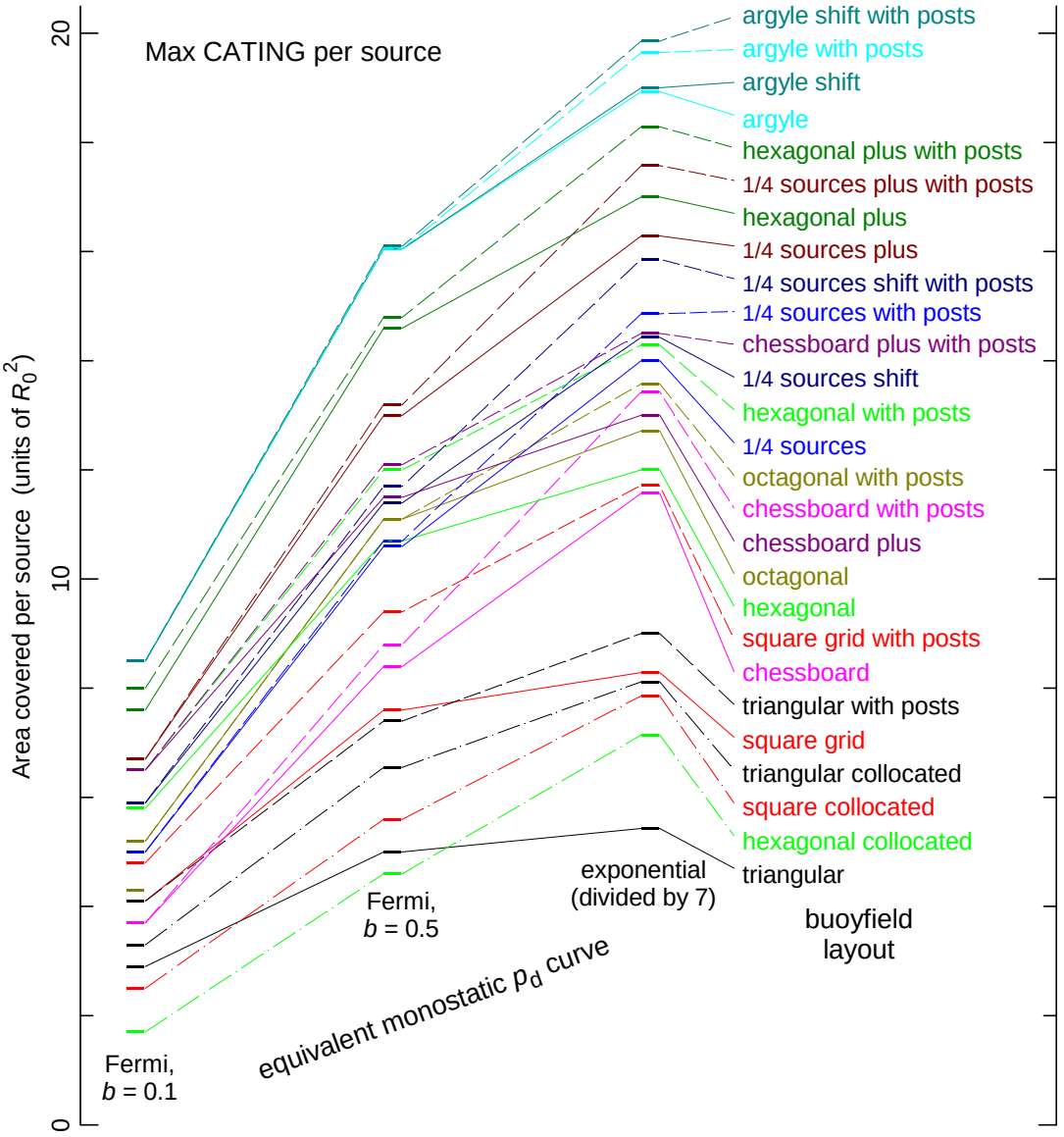

Figure 16: Max CATING per source compared across the three p_d curves. Solid connecting line – layouts with isolated sources; broken lines – with posts; chain lines – posts only (purely collocated layouts). Changes in the ordering of layouts between p_d curves occur when the connecting lines cross.

rankings, except for chessboard plus, which moves down, as does square grid and octagonal. The triangular layout performs rather badly for all three p_d curves, as do all the purely collocated layouts. Of these, triangular collocated is always best. This is the layout used in the second report in this series [2], and in the present work we have used the best network architecture of those studied in reference 2.

It is instructive to compare the collocated layouts with their corresponding separated versions (no extra receiver at each source). Hexagonal and square grid are better than their corresponding collocated layouts, but the reverse is true for the triangular layouts. This happens because of an interesting geometric property of the unit cells. Figure 8 shows that, with the same *receiver* spacing, the unit cell of the triangular collocated layout (Fig. 8a) has twice the area of the separated layout (Fig. 8b). By contrast, the unit-cell areas are equal for the square layouts (with equally spaced receivers—Fig. 3), and the benefit is reversed for the hexagonal layouts, where the collocated layout (Fig. 7c) has the *smaller* unit-cell area, at half the area of the unit cell of the separated layout (Fig. 7a). These relativities coupled with the relativities of the receivers-per-source values favour the triangular collocated layout, thereby causing it to be the only one that performs better than its corresponding separated version.

3.2 Max CATING per Sonobuoy

As could be expected, the layouts that do best in Figure 16—argyle and its variants, hexagonal plus, quarter sources plus—have many receivers per source, and those doing worst, such as the triangular, square grid and collocated layouts, have relatively few. Max CATING per source focuses on source cost and neglects receiver cost. For the opposite view, in Figure 17 we look at the max CATING per sonobuoy (rather than per source) for each layout across all three p_d curves, counting each source and receiver as a separate sonobuoy even if they are collocated.

Comparing Figure 17 with Figure 16 we see a stark difference—almost a complete reversal in the ordering of layouts, with only the octagonal layouts going against the trend. This occurs because the two metrics A_S and A_b make different implicit assumptions about receiver cost. Supposing receivers were free, we would only need to consider coverage area per source and would use the results from Figure 16. If, however, receiver and source costs were the same then we would consider the results displayed in Figure 17. It is clear that the layout deemed best depends on the relative cost of receivers to sources. For this reason, we use field cost per unit CATING as the final measure of performance.

3.3 Field Cost per Unit CATING

Field cost per unit CATING is defined in Equation (5) on p. 5. Before presenting plots of this quantity, we note an effect that allows them to be simplified. Figure 18 is a plot of field cost per unit CATING as a function of receiver cost for all of the layouts which contain either one or five receivers per source. The lines do not cross because the slope and intercept are related. As can be seen from Equation (5), the intercept where receiver cost is

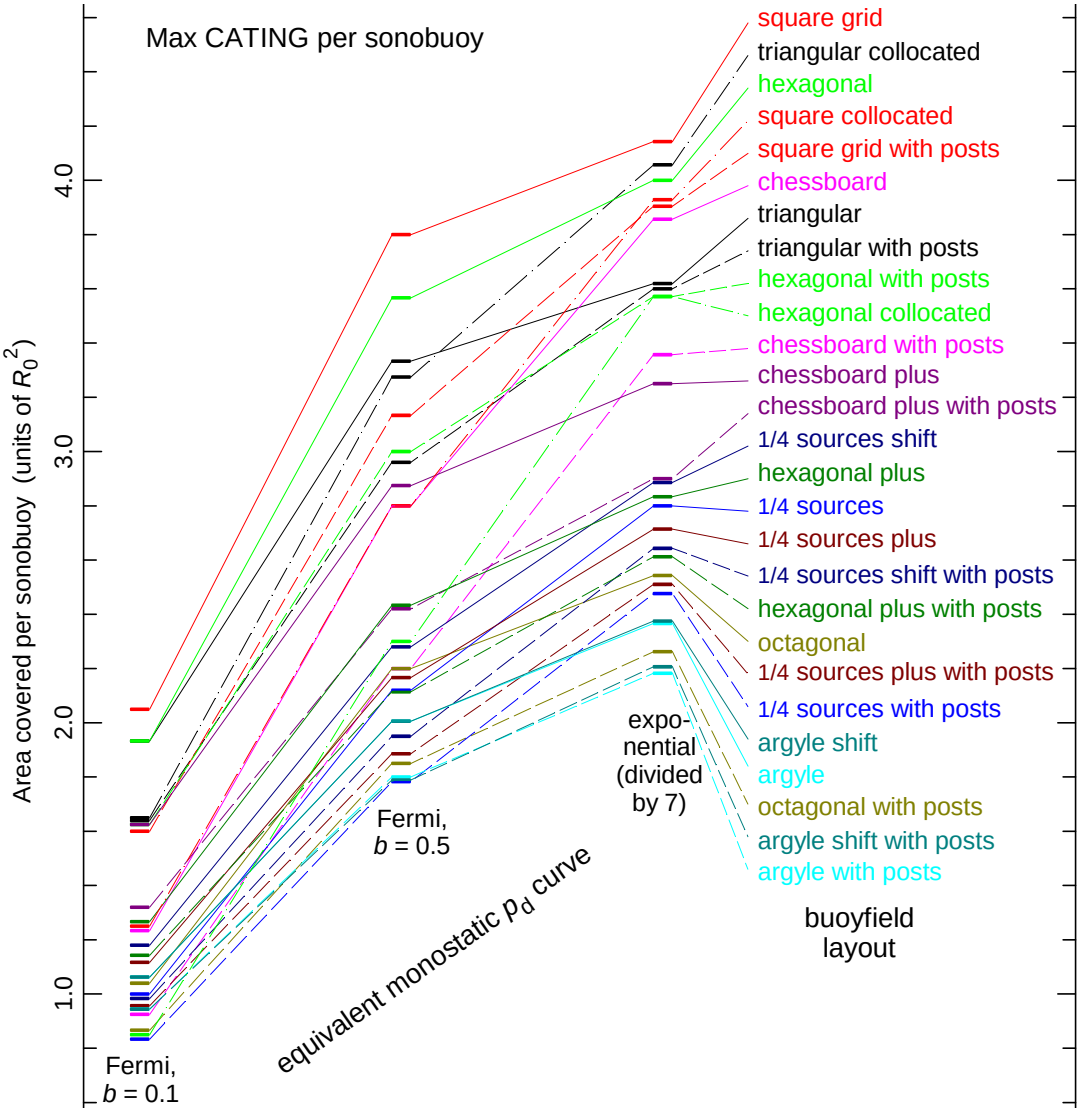

Figure 17: Like Figure 16, but for max CATING per sonobuoy with each source and receiver counting as separate sonobuoys, regardless of whether they are collocated

zero is $1/A_S$ and the slope is n_R/A_S. That is, the slope of a line increases as its intercept increases. Hence lines of layouts with the same number of receivers per source cannot cross. So, where more than one layout has the same number of receivers per source we need only consider that layout which has the highest max CATING per source. All others with the same number of receivers per source will remain consistently more expensive per unit area, increasingly so as receiver cost increases. Accordingly, we need only plot the layouts which have the highest max CATING per source for their respective number of receivers per source. These ten layouts, which are the same for all three p_d curves, are listed in Table 2.

In computing Figure 18 and compiling Table 2 we have assumed that a post costs the same as one source plus one receiver. This may need reassessing if sonobuoys with a source and a receiver in one package are available. Such a sonobuoy, if cheaper than a source sono-

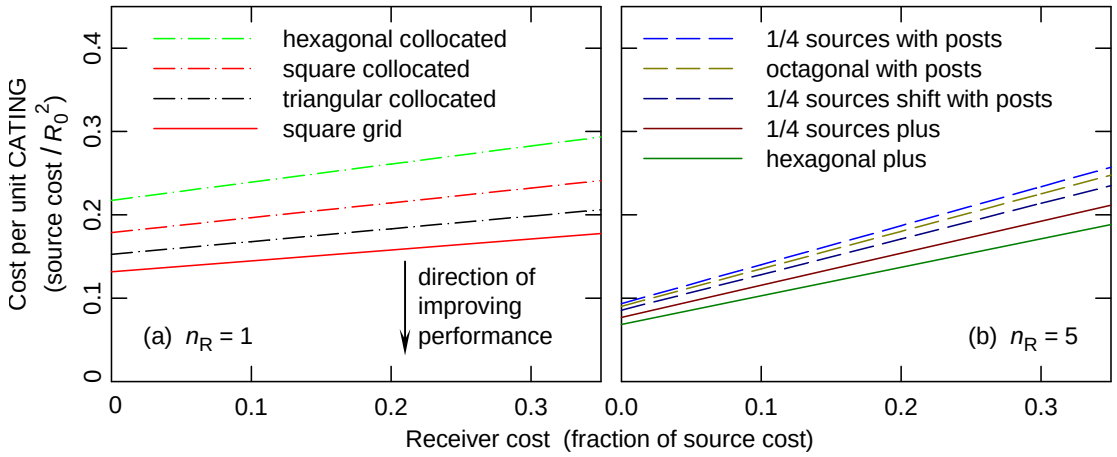

Figure 18: Cost per unit CATING as a function of receiver cost for all layouts with (a) 1:1 and (b) 5:1 receiver to source ratio (Fermi p_d *curve,* b = *0.5). Note that better performance means* lower *cost. The line colours and styles are the same as in Figures 16 and 17.*

Table 2: Layouts with the largest max CATING per source for each value of number of receivers per source. (The triangular layouts are the only ones with ½ and 1½ receivers per source.)

Number of receivers per source	Best layout
8	argyle shift with posts
7	argyle shift
6	hexagonal plus with posts
5	hexagonal plus
4	chessboard plus with posts
3	hexagonal with posts
2	hexagonal
1½	triangular with posts
1	square grid
½	triangular

buoy plus a receiver sonobuoy, would cause the collocated layouts in Figure 18(a) to move down relative to the square grid layout, but would not change their order relative to each other. It would also cause the layouts with posts in Figure 18(b) to move down relative to those without the extra receiver at each source.

Figures 19–21 compare the ten layouts to determine which are most cost effective as receiver cost varies. (Figure 21, for the Fermi p_d curve with low diffusivity, shows only nine lines because the 'argyle shift with posts' layout has the same max CATING per source as argyle shift, so its line always lies above the line for argyle shift and hence need not be shown.)

The intercepts on the y axis in Figures 19–21 are reciprocals of the values of max CATING in Figure 16, as Equation (5) indicates. Reciprocals of the values in Figure 17 would appear at receiver cost of 1.0, that is, where receivers and sources cost the same.

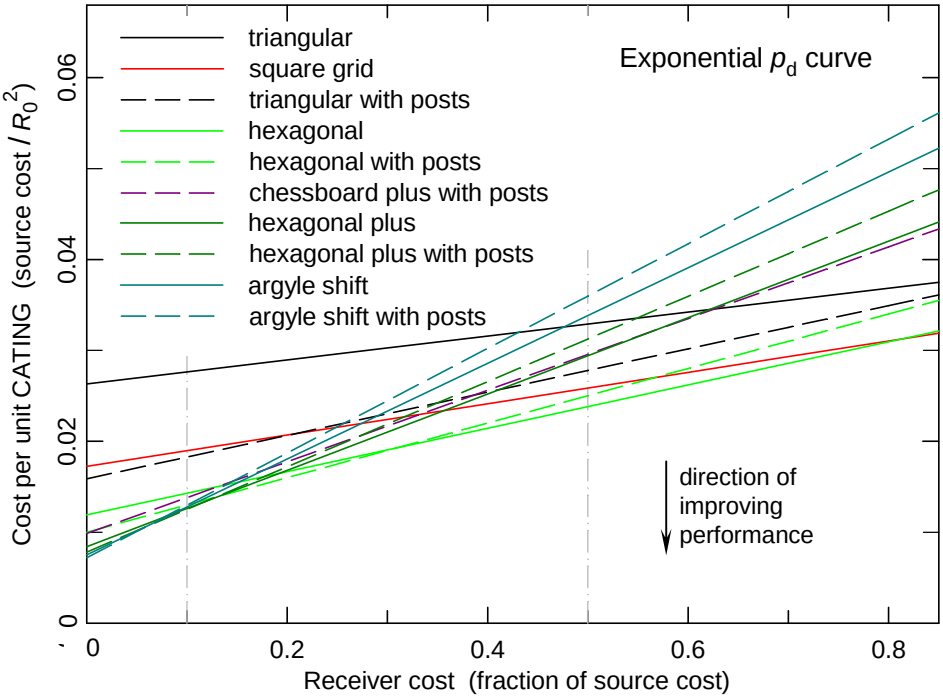

Figure 19: Field cost per unit CATING as a function of receiver cost for the exponential p_d *curve. Line colours and styles are the same as in Figures 16–18. The grey vertical lines at 0.1 and 0.5 show receiver costs of interest (see text).*

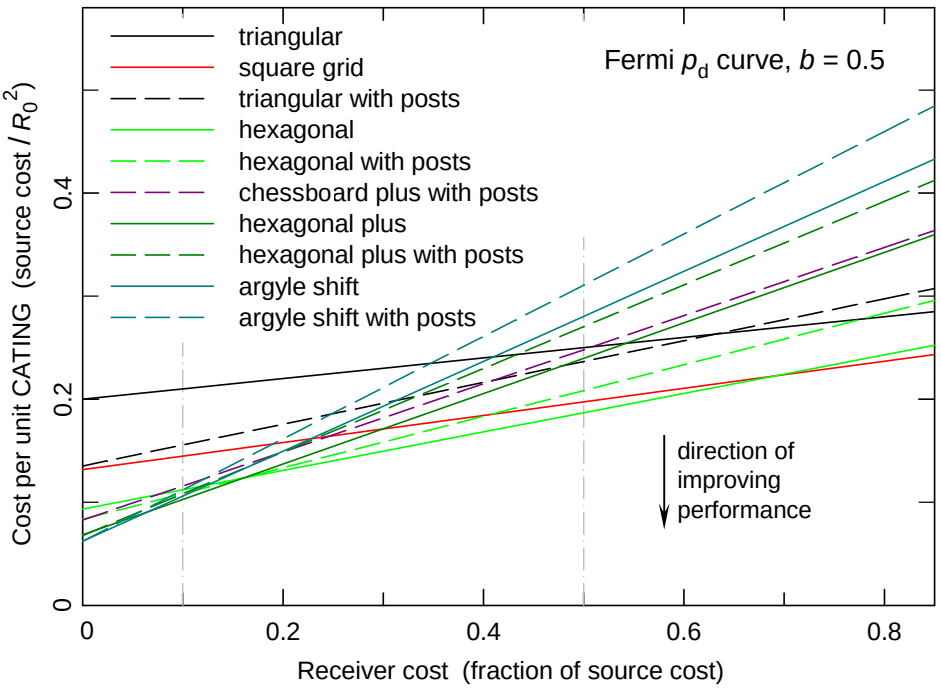

*Figure 20: As for Figure 19 but for the Fermi (*b *= 0.5)* p_d *curve*

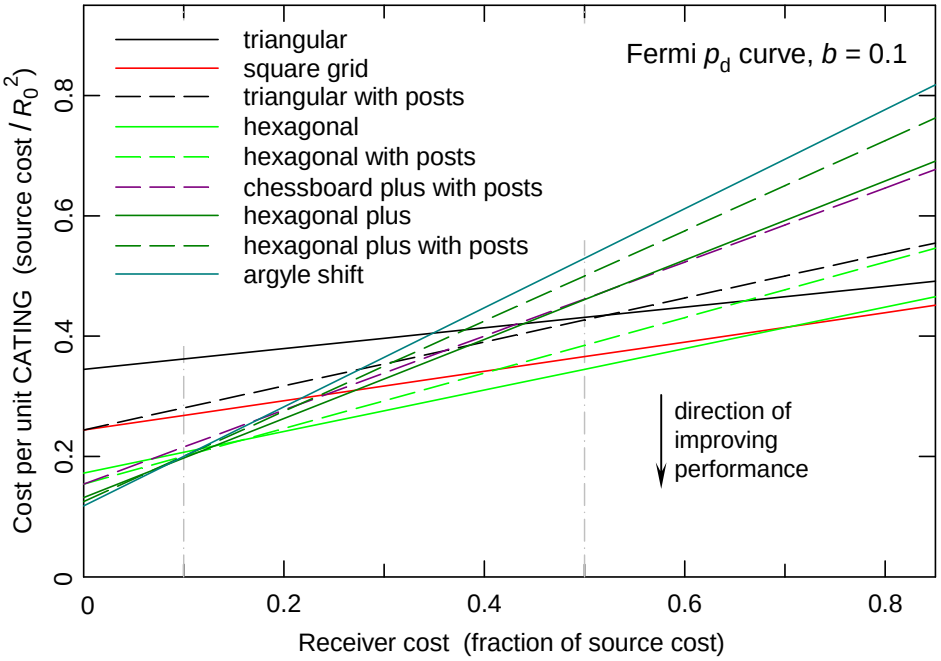

*Figure 21: As for Figure 19 but for the Fermi (*b = *0.1)* p_d *curve*

As would be expected from the area coverage data, the trend of the costing plots is similar across all three p_d curves. Each plot shows on the left-hand side the layout with the most receivers per source as best and then, as receiver cost increases, proceeds to the layout with the next lowest receiver count, skipping some out along the way. In this respect all the plots show the same trend. They differ in that the changes from one layout to another happen at different receiver cost.

The best results for an individual situation can be determined by consulting the costing plot of the relevant p_d curve at the appropriate receiver cost; however some general results can also be stated. For example:

- For sufficiently high receiver cost, the square grid is always best. The cost above which it becomes best depends on the p_d curve, but is ~0.7–0.8 times the source cost.
- Triangular layouts are never best, nor even close, except at very high receiver cost (i.e. above about 1½ times the source cost). These layouts should be avoided.
- For moderate receiver cost (i.e. about half the source cost), the hexagonal layout performs best across all three p_d curves. The wide variation we have chosen in p_d curves (Fig. 1) makes the hexagonal layout a good general-purpose choice.

Two receiver–source combinations of interest are DIFAR–AN/SSQ-125 and BARRA–AN/SSQ-125. Since the AN/SSQ-125 source is not yet in production, its eventual cost can only be estimated, but it may turn out to be ten times the cost of a DIFAR receiver and hence about twice the cost of a BARRA. That is, the BARRA–AN/SSQ-125 combination may well have a receiver cost of 0.5, so that the hexagonal layout would be recommended regardless of p_d curve, as per the last dot point above.

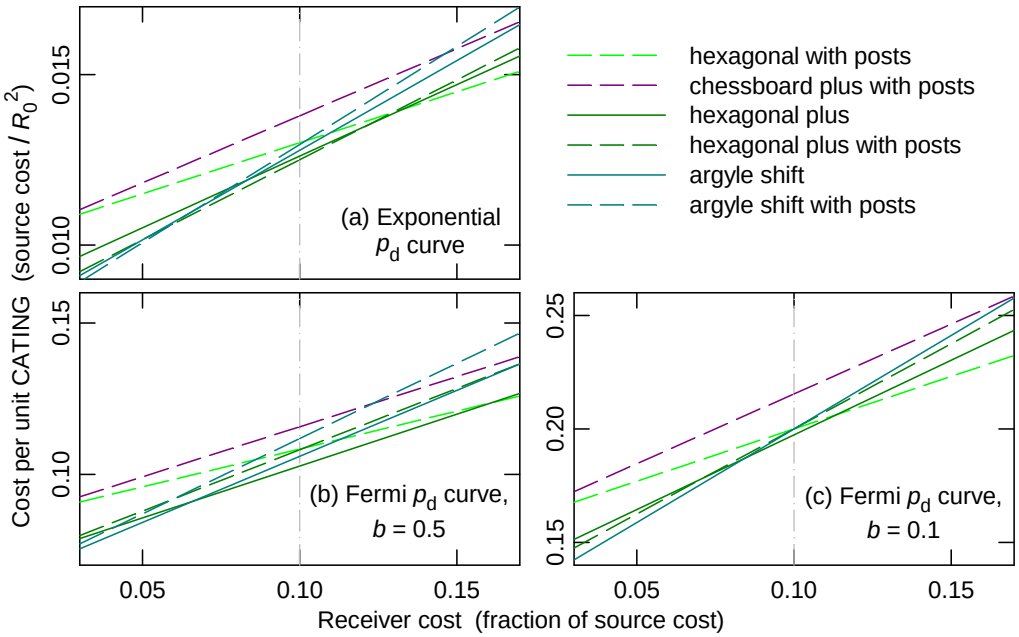

Figure 22: Detail of Figures 19–21, showing the region of receiver cost ~0.1 times source cost

For receiver cost at one tenth the source cost there is more variation between the p_d curves. Figure 22 shows expanded versions of Figures 19–21 focusing on the region around C_R equals 0.1. The best performing layout is either hexagonal plus (Fermi p_d curves) or hexagonal plus with posts (exponential p_d curve), but all the layouts shown in Figure 22 do quite well; the choice may depend on factors other than field cost as defined here.

3.4 Recommended Layouts

Figure 23 shows four of the layouts mentioned at the end of the last subsection, marked with the spacing appropriate for the high diffusivity Fermi p_d curve. The hexagonal layout is recommended for a receiver cost of about half the source cost, and the other three for a receiver cost of about a tenth of the source cost. These three give similar performance, so one could choose the easiest field of the three to be laid irrespective of p_d curve without incurring much difference in field cost per CATING. A definitive assessment of this issue should be left to those with more practical experience than us, but we envisage the fields being laid along the chain lines shown in Figure 23, in which case chessboard plus with posts (Fig. 23d) seems the easiest of the three to lay. (This is the reason for including it in Figure 23, despite it being the worst of the layouts shown in Figure 22.) Hexagonal plus involves an alternation of two row sequences, both of which are complicated. Rows of the argyle shift layout all have a repetition of seven receivers then a source, but the sources must be correctly positioned from row to row. Correct source positioning is also required for chessboard plus with posts, but the task is easier because the rows containing posts comprise a simple alternation of posts and receivers. Chessboard plus with posts covers the area with fewer sonobuoys in total than the others, but at the expense of a greater proportion of sources.

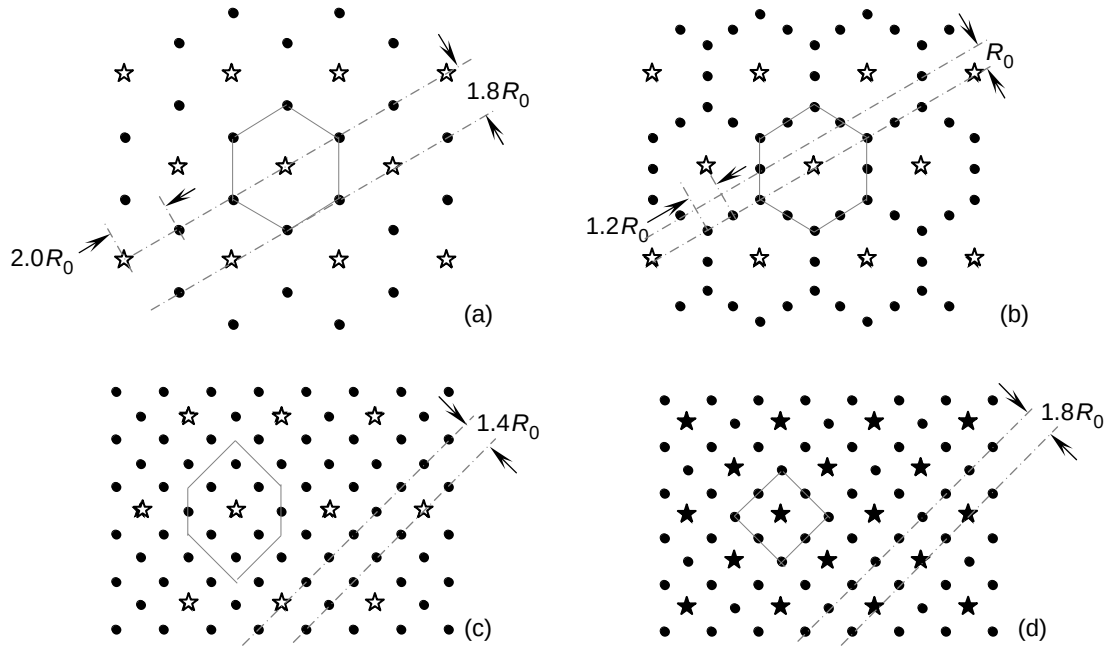

*Figure 23: Four recommended layouts: (a) hexagonal, (b) hexagonal plus, (c) argyle shift, (d) chessboard plus with posts. Sources: ☆; receivers: ●; posts: ★. The spacings marked are appropriate for the Fermi (*b = *0.5)* p_d *curve. Spacings for the other* p_d *curves are listed in Table 3.*

The spacings shown in Figure 23 apply for the Fermi (b = 0.5) p_d curve. Table 3 shows the values for the three p_d curves, all expressed as multiples of the monostatic range of the day R_0. The maximum possible spacing is smallest for a cookie cutter p_d and increases with increasing amounts of tailing in the p_d curve. It shows the extent to which the optimum spacing is influenced by the degree of tailing in the monostatic p_d curve, in addition to its dependence on R_0.

Table 3: Maximum field spacings giving full coverage for the layouts in Figure 23 and the three p_d *curves*

		Spacing (units of R_0)		
Layout		Fermi, b = 0.1	Fermi, b = 0.5	exponential
hexagonal	between rows	1.3	1.8	4.9
	between buoys	1.5	2.0	5.7
hexagonal plus	between rows	0.7	1.0	2.9
	between buoys	0.9	1.2	3.4
argyle shift	between rows	1.0	1.4	4.1
chessboard plus with posts	between rows	1.3	1.7	5.0

4. Discussion

4.1 Comparison with Other Studies

Washburn carried out a similar study more-or-less simultaneously with ours [7]. He defines an R_{equiv} in the same manner as we do (Eqn 1), but in several other important respects his method differs from ours:

- He uses a definite-range law ('cookie cutter') as the model of monostatic detection.
- Coverage area is based on detection probability rather than track-initiation probability. Multiple detections are ignored, '… since [one] detection by any source–receiver pair is sufficient for our purposes' [7(p.3)].
- His metric seeks to maximise overall coverage area, as he defines it, regardless of gaps. Consequently, his metric penalises overlapping coverage by neighbouring sensors.
- He distributes sources (or posts) and receivers randomly over the search area.

Washburn exploits these differences to obtain algebraic expressions for coverage area; corresponding expressions cannot readily be derived with our formalism. The differences between the two studies are great enough to make a detailed comparison of results pointless. For example, if neighbouring sensors do not have overlapping coverage and the detection characteristic is a cookie cutter, then it is not possible to obtain three detections in fewer than three pings, whereas this is possible in our formulation; indeed our metric favours it. (It is one reason why we avoid using an exact cookie-cutter p_{d} curve.) Washburn comments '… it would be a reasonable project to design multistatic fields that are optimal in the sense of covering the maximum equivalent area, but without the assumption that buoys are scattered randomly.' [7(p.6)] The present work can be seen as a step along this path.

Travaglione and Forward examined a field comprising one source surrounded by a circle of 2–5 equally spaced receivers [5]. As with Washburn's study, they used a definite-range law and looked to maximise coverage area based on detection probability. For the layout with 5 receivers, they find an optimum source–receiver separation of ~1.4R_0, which compares well with the values in Table 3 above for the hexagonal layout and the Fermi, b = 0.1 p_{d} curve. (Of the layouts, our hexagonal and their 5-receiver layout are closest; and the Fermi, b = 0.1 p_{d} curve is the closest we come to a cookie cutter.)

DelBalzo and co-workers have for a decade or more been developing a method of not just designing but optimising sonar search patterns taking into account the influence of a given acoustic environment [11–13], and have more recently extended the method to multistatic sonobuoy fields [14–17]. It is clear that this approach represents the desirable goal for an operational support tool. Since their algorithm optimises the location of each sonobuoy taking variations in the acoustic environment into account, it does not produce regular patterns like those studied here. This remains the case even when the acoustic environment is assumed to be uniform [15,16], presumably because of the randomness in the genetic algorithm employed. Although only obliquely hinted at in their more recent papers (e.g. [16,17]), the reader is left with the impression that the level of computational

effort required by the algorithm remains uncomfortably high. Most of their reported results involve only a few sonobuoys, although the most recent paper quotes results for as many as 16 source–receiver pairs [17], showing that calculations are possible for buoy fields of operationally relevant size.

Fox, El-Sharkawi and co-workers are also developing a buoy-field optimisation method [18–20]. Their focus is on the important question of ping sequencing, but the first paper in the series reports an algorithm for optimising sonobuoy placement. As with DelBalzo's method, they do explicit acoustic-propagation calculations and once again it appears that computation time is an issue.

Many other papers on multistatic sonar treat specific aspects of the problem—for example: localisation [21,22], track initiation [23], modelling methods [24], optimising for 'glint' detections [10,25]—but no other known to us gives an end-to-end investigation of the question of how to lay out a multistatic sonar field.

4.2 Limitations and Strengths of the Present Method

We make the following assumptions and approximations:

- Since the metric involves a type of coverage area, it refers only to detection performance. We take no account of other aspects of the operation of multistatic sonobuoy fields, such as performance in localisation, identification or tracking.
- The method of determining CATING is appropriate for large buoy fields only, for it neglects effects around the boundary of the field. In cases where a search area is small enough to be covered with a few sonobuoys, there may be better field layouts than those recommended here. For example, the 'circle-tac' layout [10], comprising a circle of receivers with a source in the centre, should be considered when the search area is small enough to be covered with a single unit cell.
- The analytical framework takes no account of time. This is typical of analyses based on coverage area. Thus, for example, submarine motion is neglected, as is the time required for all sources in the field to ping five times. This approximation is fundamentally inconsistent with that of the previous dot point: neglect of time becomes less important as the size of the field is reduced, but we explicitly consider large fields only. The development of ways of allowing simultaneous pings by several sources (e.g. [19]) would mitigate the impact of this approximation, as would the development of continuous active sonar (e.g. [26–28]), but, in view of the current state of technology, the approximation remains perhaps the most significant limitation of the present method.
- The calculation of CATING does not include dependence on target aspect angle. Since we work from monostatic p_{d} curves, the target strength is effectively an average monostatic value. In particular, we take no account the possibility of 'glint' detections by appropriately placed sensors. A recent study of the issue [10] highlighted the relative rarity of glint detections. To best exploit them, the authors recommended the 'circle-tac' field layout; our layouts closest to this are the hexagonal, hexagonal plus and octagonal.

- The definition of equivalent multistatic range R_{equiv} (Eqn 1), which is a foundation of the method, assumes power-law (e.g. spherical) spreading. This approximation is mitigated by the application of R_{equiv} to a monostatic p_{d} curve, which could include realistic acoustic propagation. That is, the use of power-law spreading affects the analysis only so far as there is a *difference* in propagation between the monostatic and multistatic geometries. This reduces its impact on the rank order of the layouts.
- The form of the sonar equation leading to the definition of R_{equiv} applies in the noise-limited regime. Acoustic-propagation calculations for the reverberation-limited regime show as much regularity as when noise-limited (e.g. compare Figs 6 & 7 in [29]), so an analysis along the lines of the analysis presented in this report should be possible by starting with the reverberation-limited form of the sonar equation (e.g. [30]).
- The method does not model false detections explicitly, effectively assuming that the false-detection load implicit in the monostatic p_{d} curve is acceptable for multistatics. This is mitigated by basing coverage area on track-initiation probability rather than single-ping detection probability, since track initiation acts as a false-detection filter. Studies and comments relating to this assumption are reported elsewhere [2,8,9,31,32].
- In calculating cost per unit CATING, we take no account of the aircraft (or other) costs in laying the field; we consider only the cost of the sonobuoys expended. Section 4.1 makes some comments on the relative ease of laying particular layouts, but we have not sought to quantify this.
- Similarly, we take no account of the effort required to monitor a receiver-rich buoy field. At some number of receivers per source, this will start to outweigh whatever cost benefit there may be in deploying more receivers.
- The max CATING values do not include any allowance for pulse compression that may reduce the size of the blind zones. We explored this for the ten best layouts and the three p_{d} curves using the method of reference 2 and a pulse-compression factor of 100.† Pulse compression never decreases the max CATING per source. The largest increase for the layouts examined is 14% (hexagonal plus, low-diffusivity Fermi p_{d} curve). In only 8 of the 30 cases computed is the increase in max CATING per source more than 5%; for 6 cases it is less than 0.1%.
- Some studies of multistatic sonar performance assume a random distribution of sonobuoys over the search area (e.g. [6,7]). A random layout would not do well with our metric because it entails random coverage-area gaps of random size. A high sonobuoy density would be needed make the probability of no gaps small. (And how small would be acceptable?) The method of determining coverage area could be adapted, but we take the view that the military would not be happy with a concept of operations that says 'scatter sonobuoys randomly over the search area'. Also, Washburn writes: 'The equivalent area covered [by an optimally designed field] would *of course* be larger than [for a random field]' [7 (p.6, emphasis added)].

†The theoretical maximum pulse compression factor is the product of pulse duration and bandwidth (e.g. [33]), which can be several hundred for frequency-modulated pulses.

The method makes no attempt to calculate the monostatic range of the day R_0. Rather than a limitation, we see this as a strength. It frees us from the complexities of multistatic acoustic propagation modelling, thereby allowing us to focus on the details of buoy-field design. By using R_0 as a universal scaling parameter, we are able to treat a diverse variety of layouts on an equal footing. Other methods of analysing multistatic sonar performance —whether detection performance or other aspects—would appear not to achieve this, judging from published accounts [6,7,10,14–25,30–39].

A second strength of the present method is the use of track-initiation probability as the route to a definition of coverage area. As mentioned above, it mitigates the neglect of the impact of false detections. However, though important, this is a secondary consideration. Its main benefit lies in providing a consistent and theoretically rigorous method for combining detection probabilities from many receivers, allowing us to take proper account of the contribution of each to the overall probability.

4.3 Posts Versus Isolated Sources

A long-standing view holds that it is always better to collocate a receiver with each source [33]. Some studies of multistatics take this further by restricting their consideration to fields composed only of posts (i.e. collocated source–receiver pairs) [14–17,29]. Washburn expresses a somewhat different view [7(p.12)]:

> 'While we have no proof of the fact, it appears from extensive experimentation that the best sonobuoy field never includes all three types [i.e. isolated sources, isolated receivers and posts], whatever the budget or costs of sources and receivers.'

His study concludes that sometimes a field of posts and receivers ('PR field') is best, sometimes one of isolated sources and receivers ('SR field'), depending on the overall budget available and the relative costs of sources and receivers. As it happens, we consider only layouts the types PR, SR and P (posts only, our 'collocated' layouts). Like Washburn, we conclude that sometimes a PR field is best and sometimes an SR field. We also agree that the relative cost of sources and receivers is a determining parameter; in our study, it is essentially the only determining parameter (Figs 19–22), since shape of p_d curve affects the results only weakly. We find no situation in which a P field is best, as Figure 18(a) shows, though this assumes that the cost of a post equals the cost of a source plus the cost of a receiver.

Our heuristic construction of candidate layouts (Section 2.3) does not naturally produce an SPR layout, that is, one with all three types of node. There seems to be no point in placing receivers at some sources and not at others. The thinking behind this view perhaps stems from our focus on large fields. Grimmett shows an example of an SPR layout (Figs 14 & 15 in [25]), the only one we have come across. It comprises a single central post surrounded by three receivers and three isolated sources alternating in a hexagonal arrangement. (Grimmett's interest in this layout concerns its ability to make 'glint' detections, and how this varies with acoustic pulse type.)

5. Conclusion

This report determines the most cost effective layout design for a field of multistatic sonobuoys using a newly developed analytical method. We test 27 layouts across three p_d curves, initially noting coverage area per source and number of receivers per source. Using these data we calculate our final measure of performance: field cost per unit area covered, where the area covered (called max CATING) is the maximum area such that track-initiation probability is greater than 50% everywhere (i.e. no coverage gaps).

The provisos in section 4.2 aside, the best layout can be determined from Figures 19–22 given the approximate shape of the p_d curve and the ratio of receiver to source cost. For example:

- For a receiver cost equal to source cost, such as when using an explosive source, the square grid layout is the most cost effective regardless of the shape of the p_d curve.
- For a receiver cost of half the source cost (approx. BARRA with AN/SSQ-125), it is the hexagonal layout which is best, again regardless of the shape of the p_d curve.
- For a receiver cost of one tenth the source cost (e.g. DIFAR with AN/SSQ-125), there are several layouts with similar costs: argyle shift, hexagonal with posts, hexagonal plus, hexagonal plus with posts and chessboard plus with posts. Which is best depends on the shape of the p_d curve, but the differences are small.
- Receiver costs need to rise to about 1½ times the cost of a source before triangular layouts become competitive. However, we have not concentrated on this part of the problem space, since we do not expect receiver cost to be higher than source cost. If this turns out to be wrong, then new layouts should be devised and tested in the manner of this report.
- If it is desired to lay a pattern of collocated source-receiver pairs only ('P field'), then the triangular arrangement is better than the square or hexagonal. This is true for all p_d-curve shapes.

These results differ somewhat from expectations, particularly in their relative insensitivity to acoustic-propagation effects—the order of the layouts depends only weakly on p_d-curve shape—and in the underperformance of layouts with posts.† This suggests further studies to explore how far the conclusions depend on the modelling choices, assumptions and approximations. For example, what would be the outcome if the 'no gaps' metric were replaced by a more traditional maximising of coverage area? What is the situation for small buoyfields? What happens in reverberation-limited conditions, or if the aspect dependence of target strength were to be included, or, indeed, if the p_d curve was obtained from acoustic-propagation modelling of a realistic environment? And so on.

† Insensitivity to acoustic-propagation effects is, of course, not a general feature of our results, but rather is obtained only through careful choice of the study question. For example, if one were to ask 'How far apart should the sonobuoys be placed?', then the answer would depend strongly on the shape of the p_d curve, as Figures 16 and 17 illustrate and the entries in Table 3 make so graphically plain. It is only when one asks 'Which layout is best?' that one finds a question the answer to which does not depend strongly on p_d-curve shape.

References

[1] S. Ozols, M.P. Fewell & J.M. Thredgold (2011) 'Track-initiation probability for multistatic sonar fields', technical note DSTO-TN-1021 of the Defence Science and Technology Organisation.

[2] M.P. Fewell & S. Ozols (2011) 'Simple detection-performance analysis of multistatic sonar for anti-submarine warfare', technical report DSTO-TR-2562 of the Defence Science and Technology Organisation.

[3] C.M. Traweek & T.A. Wettergren (2006) 'Efficient sensor characteristic selection for cost-effective distributed sensor networks', *IEEE Journal of Oceanic Engineering*, vol. 31, pp. 480–6.

[4] N.J. Willis (2005) *Bistatic radar* (2nd edn, corrected printing), Raleigh NC, SciTech Publishing.

[5] B.C. Travaglione & T. Forward (2007) 'Transmitter–receiver separation for multistatic sonar', technical note DSTO-TN-0735 of the Defence Science and Technology Organisation.

[6] M.J. Walsh & T.A. Wettergren (2008) 'Search performance prediction for multistatic sensor fields', *Proceedings IEEE Oceans 2008*.

[7] A.R. Washburn (2010) 'A multistatic sonobuoy theory', report NPS-OR-10-005 of the Naval Postgraduate School, Monterey CA.

[8] M.P. Fewell, J.M. Thredgold & D.J. Kershaw (2008) 'Benefits of sharing detections for networked track initiation in anti-submarine warfare', technical report DSTO-TR-2086 of the Defence Science and Technology Organisation.

[9] M.P. Fewell & J.M. Thredgold (2009) 'Cumulative track-initiation probability as a basis for assessing sonar-system performance in anti-submarine warfare', technical note DSTO-TN-0932 of the Defence Science and Technology Organisation.

[10] D.J. Grimmett, S. Sullivan & J. Alsup (2008) 'Modeling specular occurrence in distributed multistatic fields', *Proceedings IEEE Oceans 2008 – MTS/IEEE Kobe Techno-Ocean*.

[11] D.R. DelBalzo & K.P. Hemsteter (2002) 'GRASP multi-sensor search tactics against evading targets', *Proceedings IEEE OCEANS '02*, Biloxi, pp. 54–9.

[12] K.P. Hemsteter & D.R. DelBalzo (2002) 'Acoustic benchmark validation of GRASP ASW search plans', *Proceedings IEEE OCEANS '02*, Biloxi, pp. 60–4.

[13] D.P. Kierstead & D.R. DelBalzo (2003) 'A genetic algorithm applied to planning search paths in complicated environments', *Military Operations Research*, vol. 8, no. 2, pp. 45–59.

[14} D.R. DelBalzo, D.N. McNeal & D.P. Kierstead (2005) 'Optimised multistatic sonobuoy fields', *Proceedings IEEE OCEANS 2005 – Europe*, Brest, pp. 1193–8.

[15] D.R. DelBalzo, D.P. Kierstead & K.C. Stangl (2005) 'Oceanographic effects on optimised multistatic sonobuoy fields', *Proceedings IEEE OCEANS 2005*.

[16] G. Chacko & D.R. DelBalzo (2007) 'Tactical planning with genetic algorithms for multistatic active sonobuoy systems', *Proceedings 19th International Congress on Acoustics*, Madrid.

[17] D.R. DelBalzo & K.C. Stangl (2009) 'Design and performance of irregular sonobuoy patterns in complicated environments', *Proceedings IEEE OCEANS 2009*, Biloxi.

[18] P.N. Ngatchou, W.J.L. Fox & M.A. El-Sharkawi (2005) 'Distributed sensor placement with sequential particle swarm optimisation', *Proceedings IEEE Swarm Intelligence Symposium 2005*.

[19] D.W. Krout, M.A. El-Sharkawi, W.J.L. Fox & M.U. Hazen (2006) 'Intelligent ping sequencing for multistatic sonar systems', *Proceedings 9th International Conference on Information Fusion*, Florence, pp. 237–42.

[20] D.W. Krout, W.J.L. Fox & M.A. El-Sharkawi (2009) 'Probability of target presence for multistatic sonar ping sequencing', *IEEE Journal of Oceanic Engineering*, vol. 34, pp. 603–9.

[21] D. Grimmett & S. Coraluppi (2004) 'Sensitivity analysis for multistatic LFAS localisation accuracy', Report SR-386 of the NATO Undersea Research Centre.

[22] S. Simakov (2008) 'Localisation in airborne multistatic sonars', *IEEE Journal of Oceanic Engineering*, vol. 33, pp. 278–88.

[23] C.G. Hempel (2007) 'Track initialisation for multistatic active sonar systems', *Proceedings IEEE Oceans 2007 – Europe*.

[24] B.I. Incze & S.B. Dasinger (2006) 'A Bayesian method for managing uncertainties relating to distributed multistatic sensor search', *Proceedings 9th International Conference on Information Fusion*, Florence.

[25] D. Grimmett (2006) 'Multi-sensor placement to exploit complementary properties of diverse sonar waveforms', *Proceedings 9th International Conference on Information Fusion*, Florence.

[26] A. de Roos, J.J. Sinton, P.T. Gough, W.K. Kennedy & M.J. Cusdin (1988) 'The detection and classification of objects lying on the seafloor', *Journal of the Acoustical Society of America*, vol. 88, pp. 1456–77.

[27] B. Gillespie, K. Rolt, G. Edelson, R. Shaffer & P. Hursky (1997) 'Littoral target forward scattering', in S. Lees & L.A. Ferrari (eds) *Acoustical Imaging 23*, New York, Plenum Press, pp. 501–6.

[28] T.C. Yang (2007) 'Acoustic dopplergram for intruder defence', *Proceedings IEEE Oceans 2007*.

[29] S. Simakov, Z.Y. Zhang & L. Kelly (2009) 'Australian (DSTO) modelling methodology and cross-evaluation results', report to the September 2009 meeting of the 'Advancing Multistatic Operational Capability' workshop of Technical Panel 9, Maritime Systems Group, The Technical Cooperation Program.

[30] D. Grimmett & S. Coraluppi (2006) 'Contact-level multistatic sonar data simulator for tracker performance assessment', *Proceedings 9th International Conference on Information Fusion*, Florence.

[31] J.M. Thredgold & M.P. Fewell (2010) 'Distributed versus centralised tracking in networked anti-submarine warfare', technical report DSTO-TR-2373 of the Defence Science and Technology Organisation.

[32] J.M. Thredgold, M.P. Fewell, S.J. Lourey & H.X. Vu (2010) 'Performance assessment of sonar-system networks for anti-submarine warfare', *Proceedings IEEE OCEANS '10*, Sydney.

[33] H. Cox (1989) 'Fundamentals of bistatic active sonar' in Y.T. Chan (ed.) *Underwater acoustic data processing*, Kluwer Academic, pp. 3–24.

[34] J.I. Bowen & R.W. Mitnick (1999) 'A multistatic performance prediction methodology', *Johns Hopkins APL Technical Digest*, vol. 20, pp. 424–31.

[35] S. Coraluppi & C. Carthel (2005) 'Distibuted tracking in multistatic sonar', *IEEE Transactions on Aerospace and Electronic Systems*, vol. 41, p. 1138–47.

[36] S. Coraluppi, D. Grimmett & P. de Theije (2006) 'Benchmark evaluation of multistatic trackers', report NURC-PR-2006-007 of the NATO Undersea Research Centre.

[37] T. Lang & G. Hayes (2007) 'Evaluation of an MHT-enabled tracker with simulated multistatic sonar data', *Proceedings IEEE Oceans 2007 – Europe*.

[38] F. Ehlers, M. Daun & M. Ulmke (2009) 'System design and fusion techniques for multistatic active sonar', *Proceedings IEEE Oceans 2009 – Europe*.

[39] C.G. Hempel & J. Pacheco (2009) 'Performance analysis of the probabilistic multi-hypothesis tracking algorithm on the SEABAR data sets', *Proceedings 12th International Conference on Information Fusion,* Seattle.

DEFENCE SCIENCE AND TECHNOLOGY ORGANISATION
DOCUMENT CONTROL DATA

1. PRIVACY MARKING/CAVEAT (OF DOCUMENT)

2. TITLE

On the Design of Multistatic Sonobuoy Fields for Area Search

3. SECURITY CLASSIFICATION (FOR UNCLASSIFIED REPORTS THAT ARE LIMITED RELEASE USE (L) NEXT TO DOCUMENT CLASSIFICATION)

Document	(U)
Title	(U)
Abstract	(U)

4. AUTHOR(S)

S. Ozols and M.P. Fewell

5. CORPORATE AUTHOR

DSTO Defence Science and Technology Organisation
PO Box 1500
Edinburgh South Australia 5111 Australia

6a. DSTO NUMBER	6b. AR NUMBER	6c. TYPE OF REPORT	7. DOCUMENT DATE
DSTO-TR-2563	AR-015-023	Technical Report	June 2011

8. FILE NUMBER	9. TASK NUMBER	10. TASK SPONSOR	11. NO. OF PAGES	12. NO. OF REFERENCES
2010/1016257/1	NAV 07/338	COMFLOT	28	39

DSTO Publications Repository

http://dspace.dsto.defence.gov.au/dspace/

14. RELEASE AUTHORITY

Chief, Maritime Operations Division

15. SECONDARY RELEASE STATEMENT OF THIS DOCUMENT

Approved for public release

OVERSEAS ENQUIRIES OUTSIDE STATED LIMITATIONS SHOULD BE REFERRED THROUGH DOCUMENT EXCHANGE, PO BOX 1500, EDINBURGH, SA 5111

16. DELIBERATE ANNOUNCEMENT

No Limitations

17. CITATION IN OTHER DOCUMENTS Yes

18. DSTO RESEARCH LIBRARY THESAURUS

Sonar performance, Multistatics, Sonobuoys, Sonar detection, Track-initiation probability

19. ABSTRACT

The detection performance of a wide variety of multistatic buoy field layouts is compared using a recently developed method. The analysis applies to large area search; no consideration is given to situations where the search area can be covered with a few sonobuoys. The preferred layout depends on the ratio C_R of receiver cost to source cost. At $C_R \sim 1$, the best performing layout is a square grid; near $C_R = 0.5$ it is hexagonal; for $C_R \sim 0.1$, several layouts give comparable performance. These results hold for three different schematic monostatic detection-probability curves, ranging from almost a cookie cutter to a shape with a low-p_d tail out to several times the range of the day.